Comparison of Methods for Surface Modification of Barium Titanate Nanoparticles for Enhanced Aqueous Dispersibility and Biocompatibility

Richard Hailin Huang, [1,2,3] Nicholas B. Sobol,[4] Jason S. Lewis,[4,5,6] Rein V. Ulijn[2,3,7] and Stephen O'Brien[1,2,3]

[1]Department of Chemistry and Biochemistry, The City College of New York, 1024 Marshak, 160 Convent Avenue, NY 10031, USA

[2]Advanced Science Research Center at The Graduate Center of the City University of New York, 85 Saint Nicholas Terrace, New York, New York 10031, United States

[3]Ph.D. Program in Chemistry, The Graduate Center of the City University of New York, 365 Fifth Avenue, New York, New York 10016, United States

[4]Department of Radiology, Memorial Sloan Kettering Cancer Center, New York, NY, USA

[5]Department of Radiology and Pharmacology, Weill Cornell Medical College, New York, NY, USA

[6]Radiochemistry and Molecular Imaging Probes Core, Memorial Sloan Kettering Cancer Center, New York, NY, USA

[7]Department of Chemistry and Biochemistry, Hunter College, City University of New York, 695 Park Avenue, New York, New York 10065, United States

Abstract Colloidal barium titanate ($BaTiO_3$, or BT) nanoparticles (NPs), a type of perovskite oxides that are conventionally used as electronic materials, due to their non-linear optical properties are increasingly considered as theranostic nanocarriers. We have previously developed a facile technique to produce monodisperse BT NPs with tunable sizes between 7 to 12 nm. This size range is advantageous for the potential use of BT NPs as cancer-targeting nanoprobes owing to the enhanced permeability and retention (EPR) effect. However, BT NPs are potentially cytotoxic due to the leaching of the heavy metal ion Ba^{2+}. Moreover, surfactant-free BT NPs are poorly dispersible in aqueous solutions. To overcome these challenges, in this study, we compare and contrast three different approaches to modify the surface of our BT NPs. The first approach was to functionalize the surface of BT with a single layer of citrate *via* molecular adsorption. ## is this really a functionalization method? Does it really have an effect on the leaching issue? I wonder if it makes more sense to focus on the silica layer methods and consider this more as a control## The second approach aimed to encapsulate BT nanoaggregates

(BTNA) with a silica layer using a modified Stöber method. The third approach utilized a reverse-microemulsion method to encapsulate a single BT NP core with a thin silica layer. The -OH groups on the silica layer allowed us to further functionalize the NPs with polyethylene glycol (PEG). Our results demonstrated that each of these approaches had its own advantage and limitation; the citrate capped BT NPs exhibited extremely high dispersibility in water when the ionic strength is low ## so not really useful for biological applications; see my comment above##, whereas the silica coated BT NPs showed high stability in saline solution. Furthermore, we revealed that BT NPs are promising contrast agents for computed tomography (CT) imaging.

1. INTRODUCTION

Biomimicry or disruption of unfavorable physiological processes, signaling and treatment of disease have given rise to the development of theranostic nanomedicine, a combination of therapeutic and diagnostic goals.[1–4] Due to the range of electronic, optical and magnetic properties available, inorganic nanoparticles are attractive candidates for this purpose,[5,6] and perovskite nanocrystals are of special interest. Perovskite metal oxide materials have been extensively studied due to their tunable chemical and physical properties and wide range of applications in electronics, catalysis and photonics.[7–9] Characterized by having high dielectric constants, barium titanate (BaTiO3, or BT) is probably one of the most studied compounds of the perovskite family.[10–12]

Colloidal BT nanoparticles (NPs), on the other hand, have attracted researchers in the biomedical field to explore their application as potential theranostic nanomedicine owing to their tunable sizes, nonlinear optical properties and the high atomic number of barium.[13] The first study concerning therapeutic potentials of BT NPs was conducted in 2010 by Ciofani and coworkers.[14] This study showed that BT NPs that are non-covalently stabilized by glycol chitosan possess cytocompatibility at a concentration up to 100 μg/mL. Čulić-Viskota and coworkers[15] introduced BT NPs as second harmonic generation (SHG) nanoprobes for *in vivo* imaging in living zebrafish embryos. Most recently, Jordan and coworkers[16] reported a method to prepare antibody conjugated BT NPs which exhibit cell-specific targeting ability. In combination with other materials, BT NPs were also used for the preparation of composite scaffolds for tissue regeneration, especially as bone tissue engineering agents, owing to their piezoelectric properties.[17] Bagchi *et al.*[18] found that BT integrated poly(ε-caprolactone) (PCL) nanocomposites (BT-PCL)

significantly enhanced osteoblast proliferation and differentiation compared to neat PCL. These examples demonstrate that researchers are making progress in the exploitation of BT NPs in biomedical applications.

The use of BT NPs as either cancer therapeutic agents or imaging agents has not yet been explored. Theranostic BT NPs that are not only biocompatible in cells, but also suitable for animal studies and ultimately clinical translations, should meet three requirements. First, the NPs need to be in a certain size range to avoid fast clearance by the renal or hepatic systems. Based upon literature review and clinical observations, a 20-40 nm target size is most likely to achieve success in terms of prolonged blood circulation time, minimal liver-NP interactions and enhanced cellular internalization.[19–22] Second, the NPs should maintain colloidal stability in biological fluids. Having covalent surface coatings is crucial because electrostatically attached surface coatings tend to fail the NP colloidal stability in biological environment due to high ionic strengths.[23–25] Third, the NPs should have minimal interactions with macromolecules such as proteins and nucleic acids to avoid non-specific binding. The formation of protein corona, or broadly termed biocorona, has been known to be the ultimate obstacle for NPs to retain their functionalities or specificities after entering the biological environment.[26–28]

BT NPs with a wide range of size (3-300 nm) and crystalline phase (cubic, tetragonal, orthorhombic, etc.) can be produced through a number of synthetic routes, such as hydrothermal[29–32], solvothermal[33,34], sol-gel methods[35,36], co-precipitation[37,38] and many others[39–42]. Our group previously developed a simple and scalable sol-gel-like technique (which was referred to as the "gel collection" method) to produce monodisperse ligand-free BT NPs with tunable sizes between 7 to 12 nm.[43] This size range of BT NPs is advantageous for further surface modifications so that the final hydrodynamic size can fall within the 20-40 nm optimal range. On the other hand, the heavy atomic weight of barium makes the NPs potentially toxic in biological environments. To overcome this, it is necessary to perform proper surface modification on BT to prevent the Ba^{2+} from leaching. However, surface modifications of metal oxide NPs in this size range (sub-10 nm) have been a great challenge due to the hydrophobicity of the NP surface. Although it is one of the most common methods for SiO_2 coating, the Stöber process[44] is limited by the size, concentration and hydrophobicity of the NPs. Both small size and high concentration of the NPs can result in SiO_2 coating of aggregated cores.[45] Furthermore, due to the fast hydrolysis and condensation of the silane precursor using the Stöber process, a thickness of the SiO_2 shell below 20 nm is difficult to achieve.[46,47] A more suited SiO_2 coating method for NPs in this size range is reverse microemulsion. Although it involves a more complicated phase transfer step and usually requires a longer synthetic time, the reverse microemulsion method has been used to effectively coat a variety of

inorganic nanoparticles of size around 10 nm, with a single core-shell structure and a SiO_2 layer as thin as 1 nm.[48–51] ## all good. Given this intro it seems to me that a focus on the silica layer methods is best.

In this study, we develop and compare three different approaches to modify the surface of BT NPs synthesized by the gel collection method. These approaches include a citrate adsorption method, a silica coating by the Stöber process, and a second silica coating by reverse microemulsion. To the best of our knowledge, this is the first study concerning either citrate coating or silica coating on sub-10 nm BT NPs. We examine the colloidal stability of the post-modified BT NPs in aqueous solutions and cell media. Furthermore, we explore potential applications for each of these approaches of BT NP surface modifications and aim to provide the best strategy for their biomedical applications. By comparing the contrast ability between our surface modified BT NPs and commercial barium sulfate ($BaSO_4$) suspensions, we demonstrate here for the first time that BT NPs are potential candidates for intravenous computed tomography (CT) imaging contrast agents.

2. EXPERIMENTAL SECTION

2.1. Materials. All the chemicals were purchased from Sigma Aldrich unless otherwise stated. Milli-Q water (18.2 MΩ cm) was used in all the experiments.

2.2. Synthesis of 8 nm $BaTiO_3$ NPs. $BaTiO_3$ (BT) NPs with an average diameter of 8 nm were prepared according a previously reported method[43] with some modifications. Briefly, in a N_2 protected glove box, 5.38 mL of barium ethoxide (8.65 % w/v in ethanol) and 1 mL of titanium isopropoxide were mixed with 33.62 ml of absolute ethanol under mild stirring. After 10 minutes, 10 ml of 3:1 ethanol:H_2O was added to the mixture with continuous stirring. This process was kept for roughly 5 minutes until the mixture turned into a viscous clear solution. The viscous solution was then transferred to a closed container out of the glove box and warmed in an oven at 55 ºC for 10-24 h. A self-accumulated white solid gel monolith product was formed at this point. The monolith was then separated from the solvent, rinsed with ethanol and redispersed in appropriate amount of ethanol for further modifications. The concentration of $BaTiO_3$ NPs synthesized by this method can afford up to 50 mg/mL in absolute ethanol.

2.3. Surface modification of $BaTiO_3$ NPs by citrate adsorption, BT@Citrate. To 5 ml of as-synthesized $BaTiO_3$ NPs dispersed in ethanol at 10 mg/ml, 5 ml of 50 mM citric acid ($C_6H_8O_7$) was added while stirring. The mixture immediately turned into a cloudy solution. The stirring was stopped after 2 h followed by centrifugation at 7500 rpm for 10 minutes. The pellet was resuspended in 5 ml of citric acid and the centrifugation cycle was repeated for two more times to completely remove the ethanol. The pellet from the last centrifugation was redispersed in 5 ml of 50 mM citrate buffer at pH 7.0 to form a clear colloidal solution of BT@Citrate. The concentration of BTO@Citrate can afford up to 50 mg/mL in different buffers (pH>5.5) without signs of any precipitations.

2.4. Synthesis of silica coated $BaTiO_3$ nanoaggregates, BTNA@SiO_2

Silica coated $BaTiO_3$ aggregates, or BTNA@SiO_2 were prepared according to the Stöber method[44] with varied amounts of TEOS and water. Briefly, for the spherical BTNA@SiO_2, 9 ml of 1 mg/ml BT NPs in ethanol was mixed with 1 ml of water and 100 µL of TEOS with stirring. The mixture was stirred for 20 minutes and then 0.2 ml of ammonia solution (28%) was added to trigger the hydrolysis. The reaction was continued for 2 h until the mixture turned slightly turbid. The spherical BTNA@SiO_2 NPs were collected by centrifugation and resuspension in either water or ethanol. For the elongated BTNA@SiO_2, 2 ml of water and 50 ul of TEOS were used while the quantities of all other reagents remained the same.

2.5. Synthesis of single core silica coated $BaTiO_3$ NPs, BT@SiO_2

Single core silica coated BaTiO3 NPs were prepared following a two-step synthesis. First, the BaTiO3 NPs dispersed in ethanol was treated with oleic acid to create a non-polar surface ligand. One milliliter of BT NPs in ethanol (20 mg/ml) was mixed with 4 ml of oleic acid solution (5% v/v in cyclohexane) with stirring. The mixture was stirred for 12 h to allow the surface of the NPs to be fully covered by the oleic acids. Then the mixture was centrifuged at 13500 rpm for 20 minutes to remove ethanol and excessive oleic acids. The pellet was redispersed in cyclohexane to afford a transparent colloidal solution of BT@OA. The second step followed the reverse microemulsion method for silica coating according to literature[49]. Briefly, 0.5 ml of Igepal CO-520 was mixed with 10 mL of 0.2 mg/ml BT@OA and stirred for 10 min. Then, 0.1 mL of ammonia solution (28%) was added to the above mixture. Finally, 60 µL of TEOS was added via the equivalently fractionated drop method (adding 10 µL per 30 min). The resulting BT@SiO_2 core−shell products were collected after centrifuging and washing, and then were redispersed in either water or ethanol. By adjusting the initial concentration of BT@OA and

the amount of TEOS added in the final step, single core BT@SiO_2 NPs with average shell thicknesses between 2 nm and 20 nm can be achieved

2.6. Synthesis of BT@ SiO_2-PEG

PEGylation of BT@ SiO_2 was achieved via two steps. The BT@ SiO_2 NPs were first functionalized with amine groups. In a typical synthesis, 5 mL ethanol dispersion of 0.2 mg/mL BT@ SiO_2 NPs was treated with 5 µL of APTES and 50 µL of ammonia solution (28%). The mixture was stirred for 2 hours at room temperature. The resulting BT@ SiO_2-NH_2 products were centrifuged and washed three times to remove excessive APTES and ammonia, and finally redispersed in 5 ml of 10 mM MES buffer at pH 5.5. At this point, a significant change of the surface charge from previously negative to positive was observed. The coupling of PEG-COOH to BT@ SiO_2-NH2 was performed using the EDC/NHS strategy. In a typical synthesis, 5 mL of BT@ SiO_2-NH_2 in the above MES buffer was treated with ##

2.7. Transmission Electron Microscopy

The TEM images were taken on FEI Titan Themis 200kV TEM (USA). For all TEM samples, 5 µL of appropriate BT solution was drop casted on a Formvar/carbon film grid (300 mesh, copper; TED PELLA, USA). The grid was then dried at room temperature overnight before examining.

2.8. Fourier Transform Infrared Spectroscopy

The FTIR spectra were acquired from 4000 to 500 cm^{-1} with 64 scans at 4 cm^{-1} resolution on a Bruker Vertex 70 spectrometer (USA). BT in ethanol samples and BT@Citrate aqueous samples were lyophilized and dried in an oven at 70° C overnight. FTIR pellets were prepared after homogeneous mixing of the dried samples with KBr. The background was corrected by a reference of KBr pellets.

2.9. Hydrodynamic Diameter and ζ-Potential Measurements

The hydrodynamic diameter and surface charge were recorded with Anton Paar Litesizer 500 Particle Analyzer (Austria). For the particle size measurements, 1 mL of 0.1 mg/mL BT or surface modified BT samples were placed in quartz cuvettes. The volume weighted size distribution peak values were used to report the hydrodynamic diameters of samples. For the ζ-Potential Measurements, 0.3 mL of 0.1 mg/ml aqueous solutions of BT@Citrate, BT@SiO_2, BT@SiO_2-NH_2 or BT@SiO_2-PEG were injected in Omega cuvettes. The Smoluchowski approximation was selected to calculate the ζ-Potential values.

2.10. UV-Vis Spectroscopy

The UV-Vis absorption spectra of the BT NPs in ethanol were recorded on JASCO V-660 UV-Vis Spectrophotometer (Germany) using quartz cuvettes with 1 cm path length.

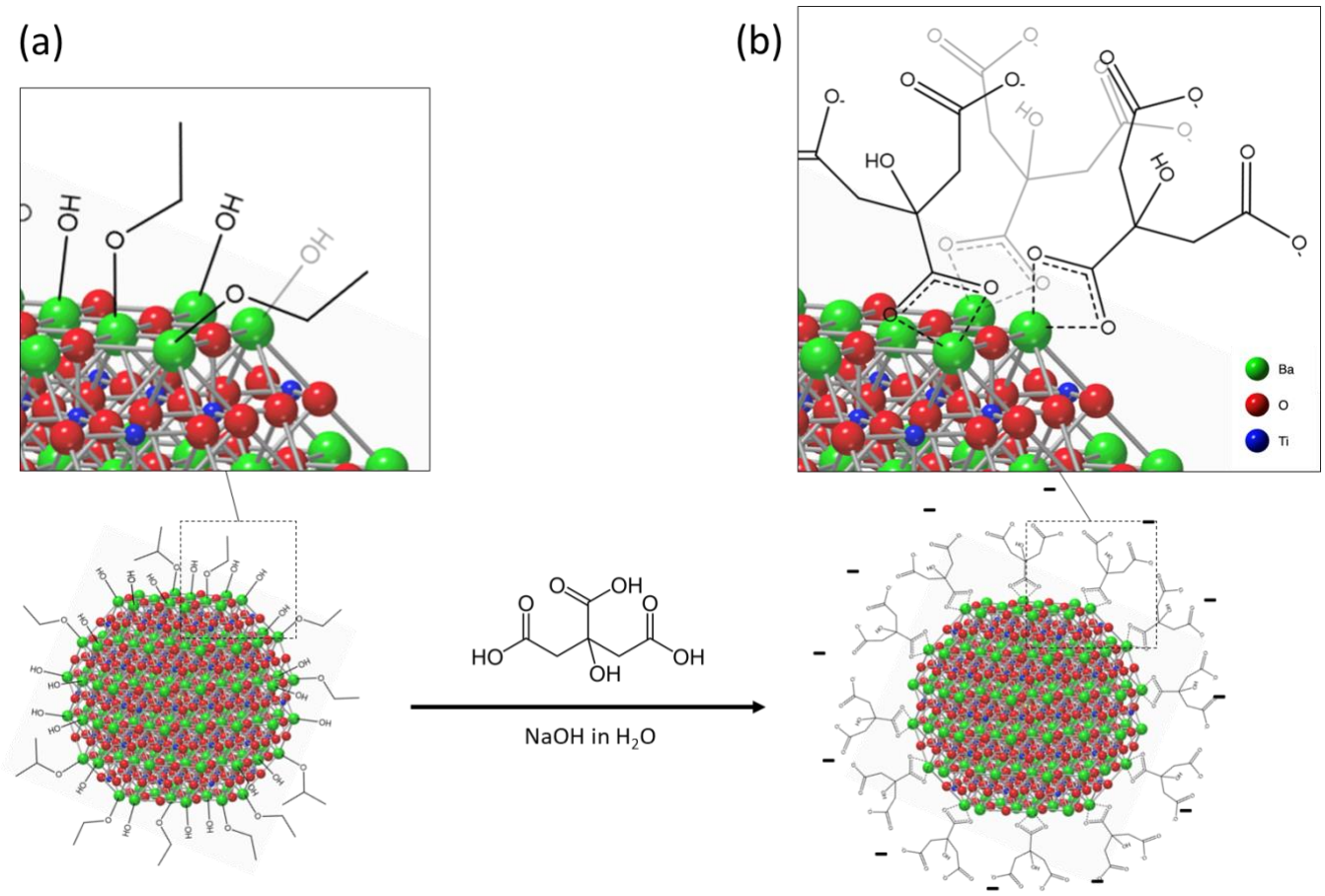

Figure 1. Schematic illustration of BT@Citrate synthesis. (a) surface chemistry of BT NPs prepared by the "gel collection" method; (b) surface chemistry of as-synthesized BT@Citrate NPs.

3. RESULTS AND DISCUSSION

3.1. Nanoparticle Characterization

3.1.1. BT@Citrate. As-synthesized BT NPs with an average diameter of 8 nm using the "gel collection" method were found to be highly dispersible in polar organic solvents such as ethanol and furfuryl alcohol, but poorly dispersible in non-polar organic solvents or water. This result can be explained by their surface chemistry which is abundant in hydroxy and ethoxy groups.[43] Citrates play an important role as a surface capping agent and stabilizer in many synthetic routes of inorganic NPs,[52–54] with the most well-known ones being the syntheses of gold and silver NPs.[55,56] Herein we used citrate as a post-synthesis surface capping agent to enhance the colloidal stability of BT NPs in water. Figure 1 illustrates the change of surface chemistry on BT before (Figure 1a) and after (Figure 1b) the citrate

adsorption. The FTIR spectra in Figure 2d confirm that the citrate molecules were adsorbed on the surface of BT@Citrate, as indicated by the emerging peaks at 1562 cm^{-1} and 1392 cm^{-1}, which are the characteristic peaks arising from the asymmetric and symmetric stretching of the carbonyl groups (C=O) on carboxylates (COO^-). The photographs in Figure 2c also reveal that the BT@Citrate NPs dispersed in water formed a transparent colloidal solution, while the BT NPs in water clearly settled at the bottom of the solution. These results demonstrate that the BT NPs suspended in water are not irreversibly agglomerated and can be surface functionalized in order to attain a high degree of dispersibility, towards a highly stable colloidal solution (Figure 2c). The small size (8.3 ± 0.3 nm) of BT is likely critical in this regard. The citric acid ($C_6H_8O_7$) solution that is added to the colloidal BT solution in ethanol is partially deprotonated ($pK_{a\,1}$ = 3.13, $pK_{a\,2}$ = 4.76, $pK_{a\,3}$ = 6.4) to yield a mixture of citric acid molecules and citrate ions. The dispersibility of the BT@Citrate NPs was found to be highly pH dependent. When the pH of the dispersion falls below 4.8, the transparent colloidal solution started to get cloudy, indicating the agglomeration of BT@Citrate NPs. As the pH was increased again to pass 5.5, the cloudiness disappeared, and the solution turned back to transparent. This reversible transition of pH dependent dispersibility was shown in the video in Supporting Information. The TEM images of the samples in Figure 2c before and after citrate modification are shown in Figure 2a and 2b. As shown, the BT NPs was agglomerated to a certain degree, while the BT@Citrate NPs remained well-dispersed.

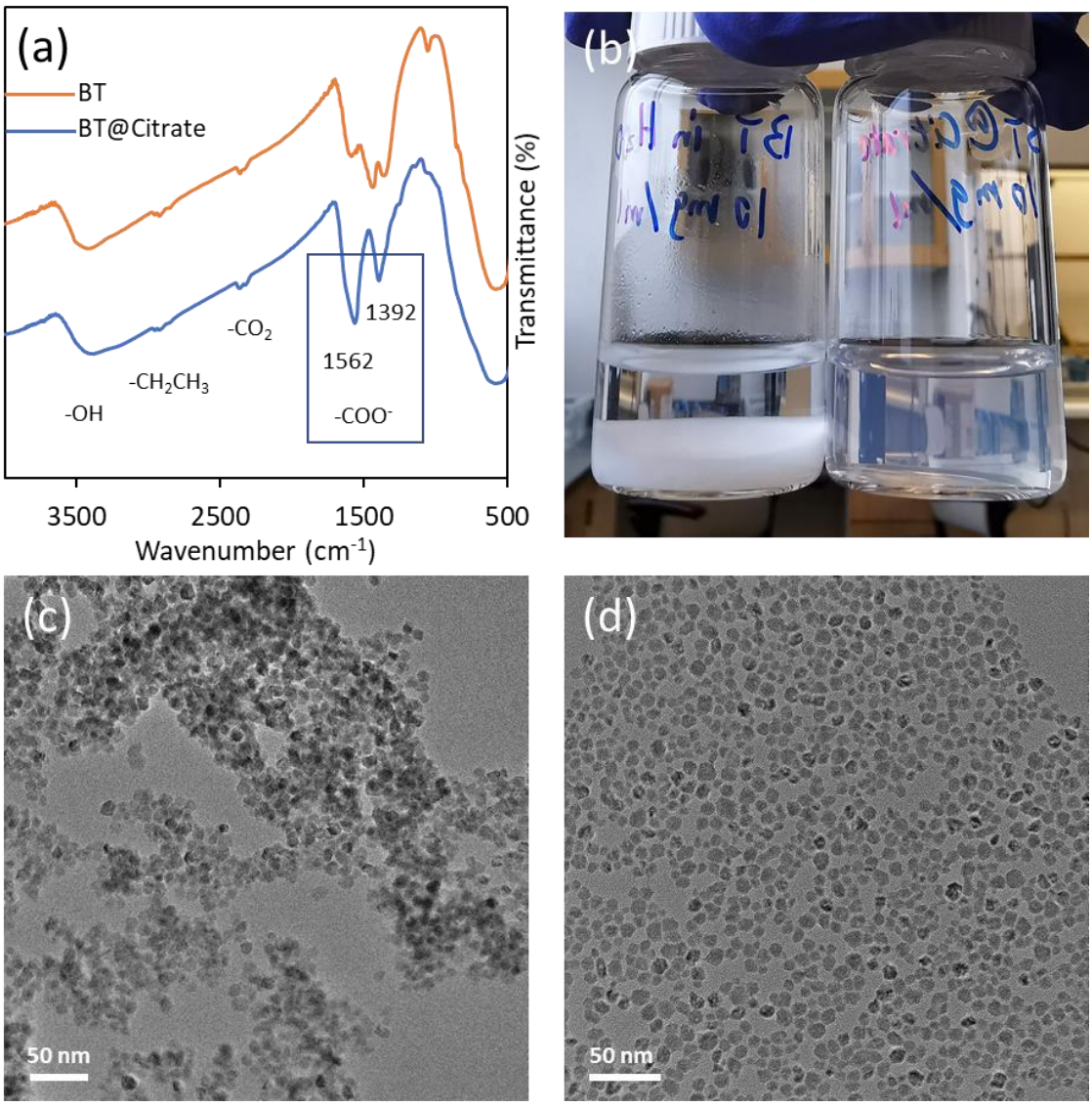

Figure 2. Characterizations of BT@Citrate NPs. (a) FTIR spectra of BT (top) and BT@Citrate (down). (b) Macroscopic photographs of BT in water (left) and BT@Citrate in water (right). ## consider cropping## (c) and (d) TEM images of dried samples of BT and BT@Citrate NPs.

3.1.2. BTNA@SiO_2. BTNA@SiO_2 NPs were synthesized using a modified Stöber method.[44] Figure 3a illustrates the synthesis scheme of the silica coating on BT NPs. It is important to note here that the BT aggregates resulted from the addition of H_2O during the silica coating synthesis. The average thickness of the silica shell of BTNA@SiO_2 is tunable between 20 – 100 nm by adjusting the amount of TEOS. A large thickness (100 nm) and smooth surface of silica shell is achieved by increasing the amount of TEOS to 100 µL to coat 9 mL of 1 mg/mL BT NPs. Figure 3b shows the TEM image of

spherical BTNA@SiO_2 NPs with an average silica shell thickness of 90 nm. The size of the BT aggregates core and the morphology of the silica coated NPs can be tuned by changing the ethanol/H_2O ratio. As-synthesized BT NPs using the gel collection method were highly dispersible in polar organic solvent such as ethanol and furfuryl alcohol, but poorly dispersible in H_2O. However, H_2O is one of the key reagents in the Stöber process. As such, aggregation of BT NP during prior to the coating is inevitable and the degree of aggregation of the NPs is dependent on the ethanol/H_2O ratio. Elevated concentration of H_2O also leads to inhomogeneous nucleation of SiO_2 on the BT surface, creating rough and nonuniform silica surfaces.[57,58] The elongated or irregular shape of BTNA@SiO_2 with large cores was observed by adding a high concentration of H_2O (ethanol/H_2O < 4). Figure 3c shows the TEM image of elongated BTNA@SiO_2 NPs with an average silica shell thickness of 20 nm. As shown, the morphologies of both the BT core and the silica shell structures differ greatly from the spherical BTNA@SiO_2. Elemental composition of the core-shell structure of BTNA@SiO_2 NPs was confirmed using Energy-dispersive X-ray spectroscopy (EDS) (Figure 3d).

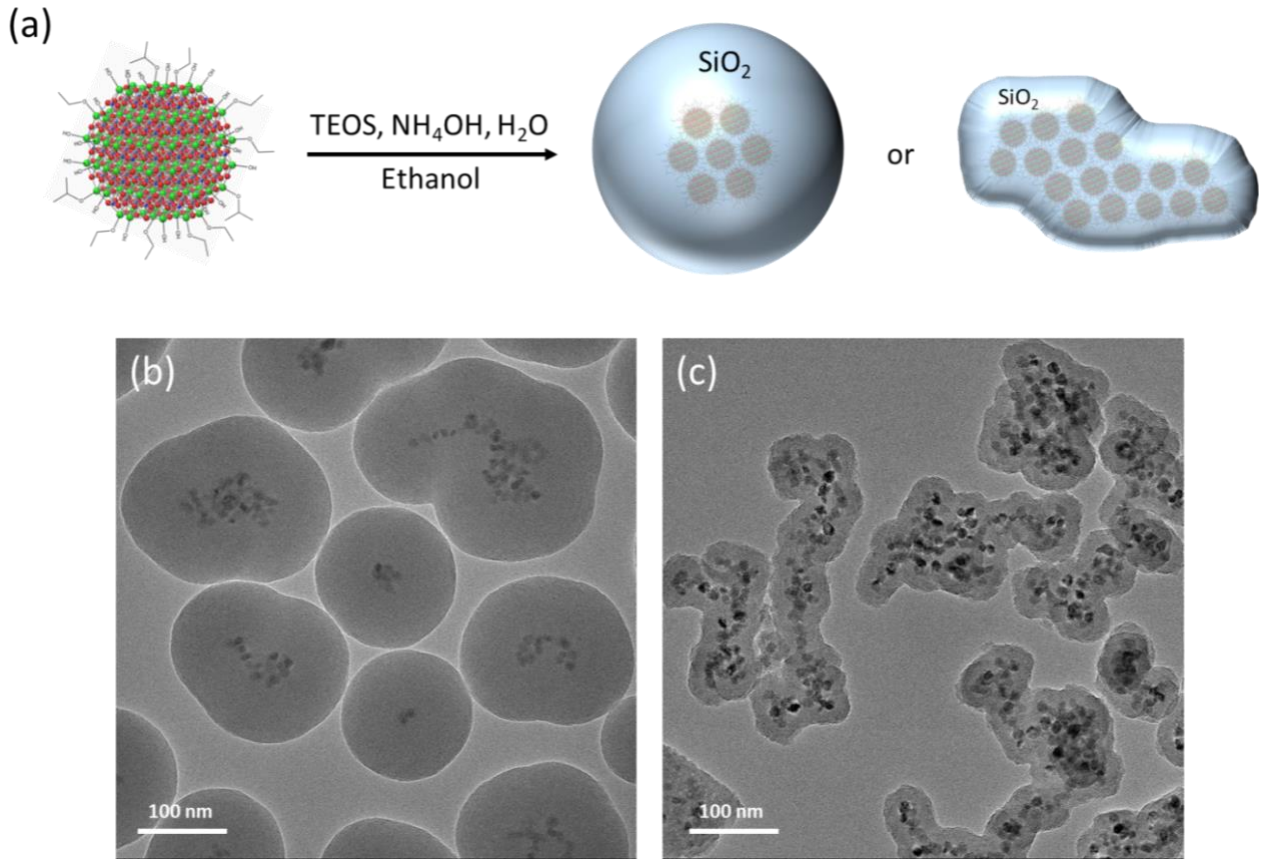

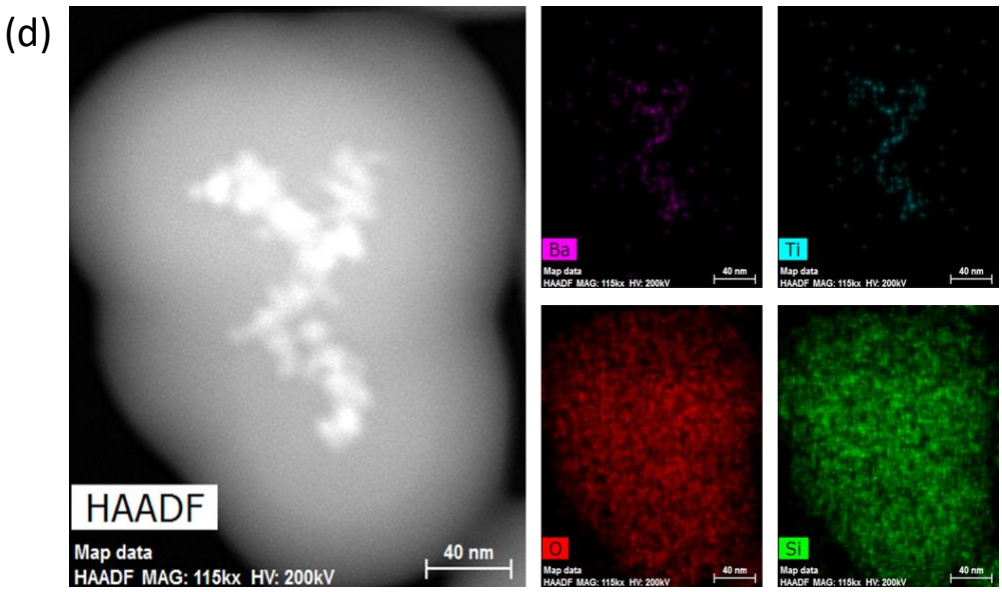

Figure 3. (a) Synthesis scheme of silica coating of BT aggregates. The shell thickness and the size of the BT aggregates core can be well controlled by changing the amounts of TEOS and H_2O added in the synthesis. (b) and (c) TEM images of spherical BT(aggregate)@SiO_2 and elongated BT(aggregate)@SiO_2. (d) Energy-dispersive X-ray spectroscopy (EDS) mapping of BTNA@SiO_2.

3.1.3 BT@SiO_2. A schematic illustration of a multi-step synthesis of BT@SiO_2 from BT NPs is shown in Figure 4a and 4b. It involves first a solvent transfer from ethanol to cyclohexane using oleic acid (OA) which is followed by a reverse microemulsion process for silica coating. Figure 5a shows the TEM image of well-dispersed BT@OA NPs after the solvent transfer of BT from ethanol to cyclohexane. This is critical step to prevent encapsulation of multiple particles per silica shell due to mild agglomeration of BT NPs. With the carboxylate group adsorbed on the BT surface, the long hydrocarbon chain of OA allows the NPs to achieve a high dispersibility in non-polar solvents such as cyclohexane. This step was essential because the reverse microemulsion method for silica coating was applied to achieve a shell thickness of less than 10 nm. Figure 5b shows the TEM image of the BT@SiO_2 NPs produced by this method with an average shell thickness of 9 nm. As shown, most of the NPs have a single BTO core except a few others that encapsulated two or more BTO NPs. This demonstrates that even though the BT@OA NPs are highly dispersed in cyclohexane, there still exists

dynamic interactions between each NP causing the silica nucleation to occur when two or more NPs are close together.

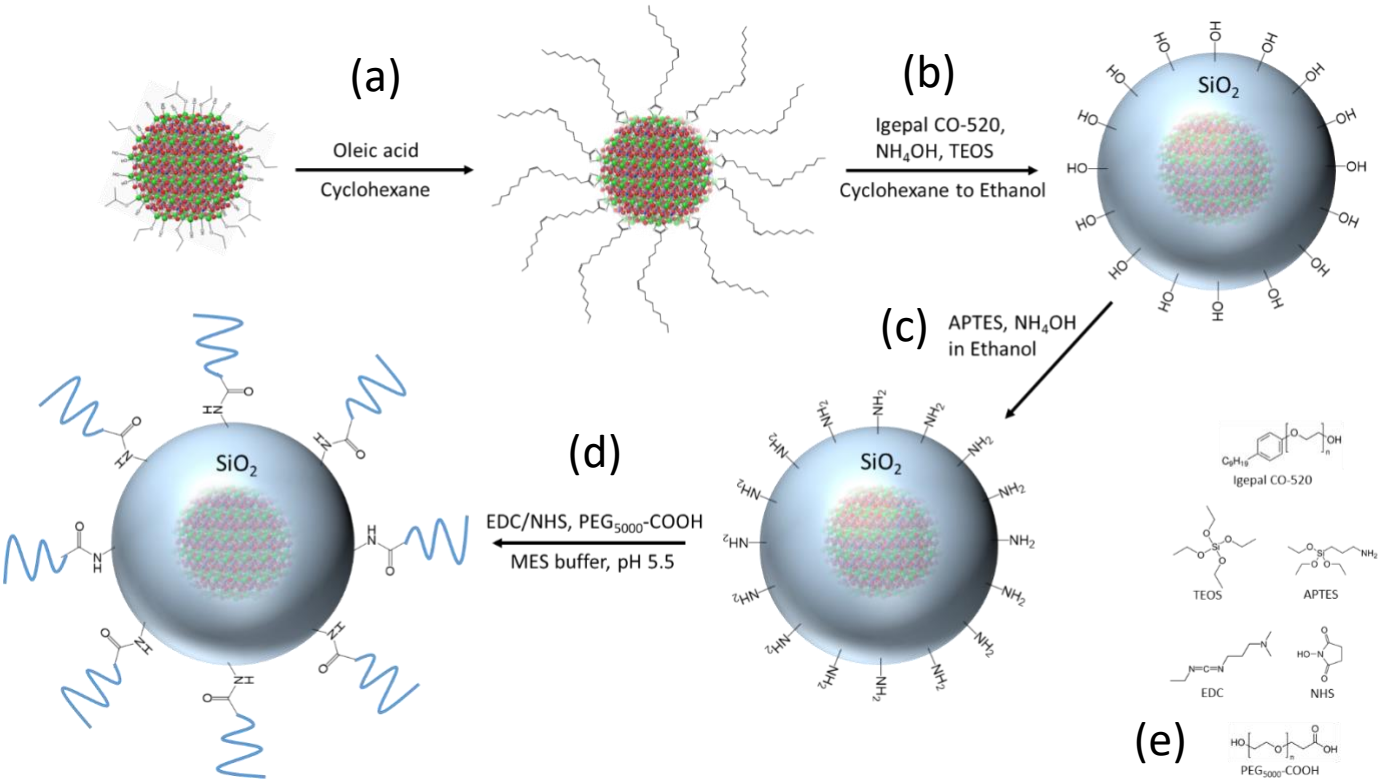

Figure 4. Multi-step synthetic route of BT@SiO_2-PEG NPs from BT NPs. (a) Transfer of the NPs to a non-polar solvent using oleic acid as surface ligands; (b) silica coating via the reverse microemulsion method; (c) surface amination using APTES; (d) surface PEGylation by EDC/NHS coupling. (e) Chemical structures of different reagents used.

3.1.4. BT@SiO_2-PEG. The surface of BT@SiO_2 was further covalently coupled with polyethylene glycols (PEGs). A schematic illustration of a multi-step synthesis of BT@SiO_2-PEG from BT@SiO_2 is shown in Figure 4c and 4d. APTES was used to activate the silica surface on BT@SiO_2 NPs so that the particles become coated in reactive amine groups that are readily available for EDC/NHS coupling with PEG-COOH. The EDC/NHS set is one of the most commonly used coupling reagents to catalyze the amide bond formation between carboxyl and amine groups for water-soluble NPs.[59–63] The TEM images of the amine functionalized BT@SiO_2 NPs (BT@SiO_2-NH_2) and the PEGylated BT@SiO_2 NPs

(BT@SiO_2-PEG) are shown in Figure 5c and 5d, respectively. It can be noticed that the BT@SiO_2 (Figure 5b) and BT@SiO_2-NH_2 NPs were slightly more agglomerated compared to the BT@SiO_2-PEG NPs. This suggested that PEGylation indeed enhanced the aqueous dispersibility of the BT NPs.

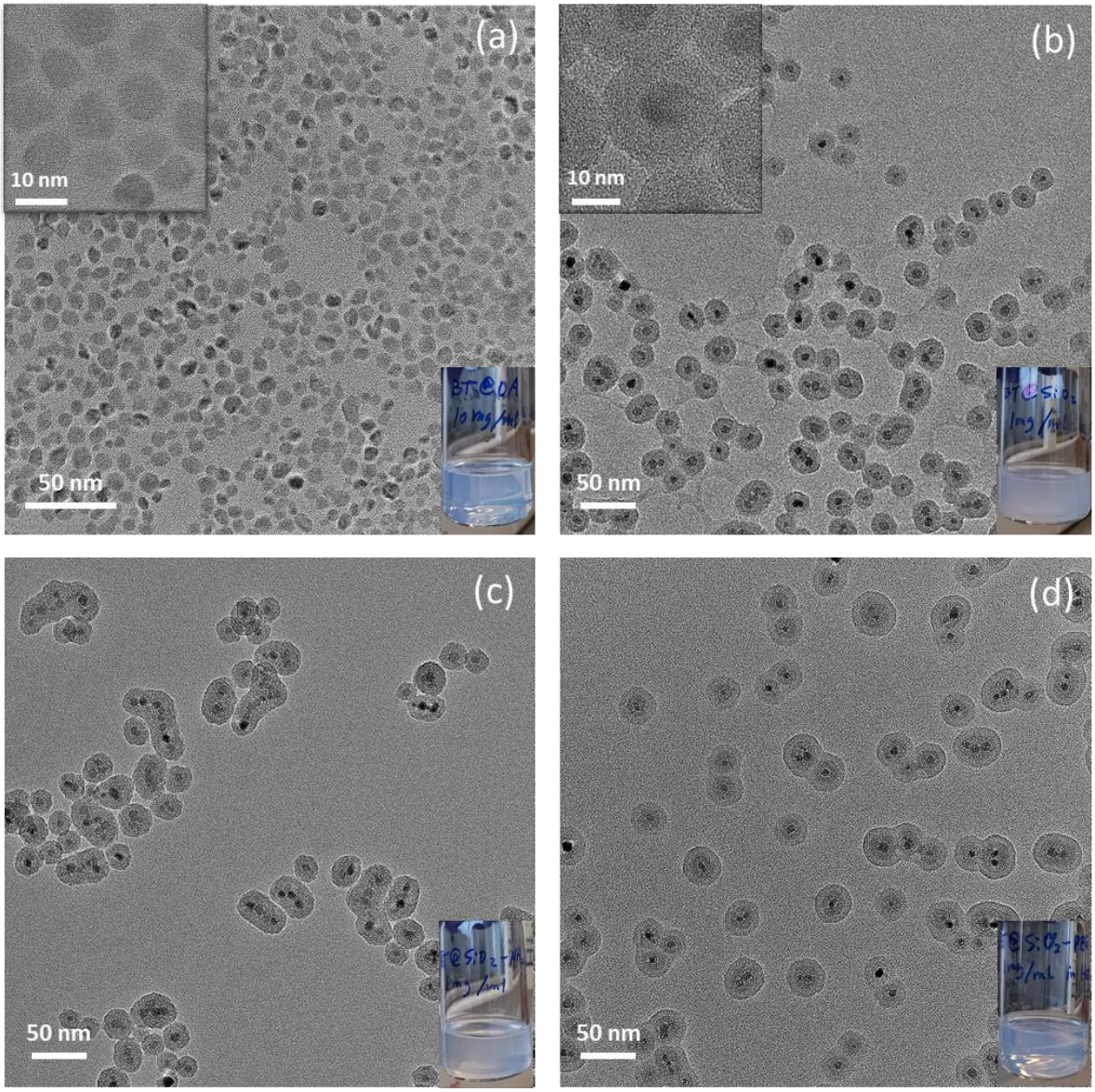

Figure 5. TEM images of (a) BT@OA, (b) BT@SiO_2, (c) BT@SiO_2-NH_2 and (d) BT@SiO_2-PEG. The top left insets in (a) and (b): magnified TEM images of each sample. Bottom right insets: photographs of each sample in their appropriate solvent. (a) BT@OA in cyclohexane; (b) BT@SiO_2 in ethanol; (c) BT@SiO_2-NH_2 in ethanol; (d) BT@SiO_2-PEG in water.

3.2. Biocompatibility of BT NPs

The application of BT NPs for biomedical purposes, especially as therapeutic and diagnostic nanomaterials, is relatively recent. To date, pristine BT NPs produced by most of the synthetic routes[34–47], including the gel collection method[43], are not biocompatible in terms of their aqueous stability and cytotoxicity . BT is known to be thermodynamically unstable in aqueous environment due to the leaching of Ba^{2+} at low pH or the formation of $BaCO_3$ at high pH.[35,64,65] In this study, all three coating methods produced highly stable BT NPs in water (Figure 2, 3 and 5). Among these methods, the BT@Citrate NPs can achieve the highest concentration in aqueous solutions (up to 50 mg/mL) without signs of precipitation. To the best of our knowledge, this is the first study to report such high dispersibility of colloidal BT NP in aqueous solutions. The colloidal stability of BT@Citrate is largely affected by the ionic strength in the aqueous solution. At high NaCl concentration (>50 mM), the BT@Citrate dispersion started to turn turbid and settle over time. This suggested that the citrate adsorption on the surface of BT is dynamic and can be disrupted or replaced by a high concentration of ions or ligands. In this respect, the citrate-NP interactions on BT@citrate behave in a similar fashion as the widely studied citrate capped gold nanoparticles that they start to aggregate upon a threshold of salt concentration.[23,66,67] It is therefore clear that even the BT@citrate NPs possess high dispersibility in water, the nature of the relatively weak electrostatic interaction between the coating ligand and the surface will eventually fail to maintain colloidal stability in biological fluids. Nonetheless, this post-synthetic citrate treatment can be applied to many other doped derivatives[43] of BT NPs prepared by the gel collection method. The BTNA@SiO_2 and BT@SiO_2 NPs, in contrary, did not exhibit as high dispersibility in water as did BT@Citrate. These silica coated NPs started to turn turbid and settle overtime as soon as the concentration reached to approximately 5 mg/mL. Below 5 mg/mL, the NPs maintained homogeneous dispersity in aqueous buffer solution even at saline concentration (150 mM). For the BT@SiO_2-PEG NPs, the colloidal stability remained high without signs of settling at a concentration up to 10 mg/mL. Indeed, the BT@SiO_2-PEG NPs showed the most potential to become theranostic agents as they meet the three requirements stated in the introduction to some degree. These NPs have an overall size of slightly larger than 40 nm; they maintain colloidal stability at saline concentration which resembles the condition in biological environments; and they are functionalized with non-fouling PEG chains.

It has been shown that the leaching of Ba^{2+} on BT surface has a high dependency on the pH of the solution, with higher and faster leaching rate at lower pH.[65,68] As a result, the surface of BT will become rich in TiO_2 and hence it will promote NP aggregation at low pH. In the case of our BT NPs, after the citric acid treatment, immediate precipitation of the NPs was observed. This could be caused by two different scenarios. First, the surface Ba^{2+} ions were likely to be stripped giving rise to a TiO_2-rich surface. The subsequent addition of NaOH deprotonated the citric acids to form citrates, which in turn formed metal complex bonds with Ti (IV). Thus, the NPs were dispersed due to electrostatic repulsion. Alternatively, the citric acid formed metal complex bonds directly with the surface Ba (II) which, contrarily, was stabilized. ## XPS?## While the precipitation was caused by hydrogen bonding between the carboxylic acids on adjacent NPs, ## evidence?## the addition of NaOH deprotonated the acids to form electrostatically repulsed carboxylates on the citrates on the NP surface. A similar study was performed on 50 nm barium strontium titanate (BST) NPs by first using nitric acid to remove the surface Ba^{2+} and subsequent treatment with citric acid for surface adsorption.[69] In our study, however, treating the small BT NPs (<10 nm) caused a significant size reduction of individual NP and also random aggregation of some NPs due to the TiO_2 rich surface. Thus, direct citric acid treatment was used in our study. Without enough evidence, further studies will be required to fully understand the nature of the interaction between the citrate molecules and the surface of BT.

3.3. BT NPs as contrast agents for computed tomography (CT)

Computed tomography (CT) is a non-invasive tissue imaging technique employed in numerous research and clinical settings.[70,71] Barium has long been known to be of great value in highlighting the area of interest in CT imaging. Barium sulfate ($BaSO_4$) suspension has been the predominant contrast agent for improving the visualization of CT imaging of the gastrointestinal tract. The reason why Barium is excellent for CT imaging is multifold ##or complicated?##. Due to the high atomic number, Z, of Barium, the position of its K-shell electron absorption edge (*k*-edge, ~39 keV), i.e., the photon energy at which Barium has the highest attenuation, overlaps with the distribution peak of the X-ray energy produced by clinical CT scanners (typically operate at a voltage between 80-140 kV).[72] This means that barium absorbs more photons than other elements do from the X-ray produced by clinical CT scanners. Moreover, barium is abundant and $BaSO_4$ is relatively cheap to produce. CT is an extremely useful, low-cost and routine technique, but lacks the level of contrast and resolution, when compared to

MRI/PET, and it has been speculated improved contrast enhancement would greatly benefit the medical profession.[73]

CT relies on the X-ray attenuation properties of different materials to achieve imaging effectiveness. For example, bones appear much brighter than lungs do in a CT scan because X-ray attenuates (being absorbed) on bones much more than on lungs. In general, tissue with higher density (ρ) or higher atomic number (Z) tend to better absorb X-rays.[73] The degree of X-ray attenuation on different materials, or X-ray absorption coefficient (μ), and is expressed as

$$\mu = \frac{\rho Z^4}{AE^3}$$

where A is the atomic mass and E is the X-ray energy. Figure S1, shows a chart of attenuation coefficient vs. photon energies of different elements to illustrate the utility of Barium. A CT scan uses a standardized scale to measure the ability of tissues to attenuate X-ray in Hounsfield units (HU). By definition, water is assigned to have a value of 0 HU, so that the CT scanners can be calibrated with a reference to water. For a material with a linear X-ray attenuation coefficient "μ" the corresponding HU value is calculated by

$$\mathrm{HU} = \frac{\mu - \mu_{water}}{\mu_{water}} \times 1000$$

where μ_{water} is the X-ray attention coefficient of water. Many soft tissues, e.g., livers and spleens, share similar HU values as they are made of mostly water. As such, contrast agents with relatively higher HU are usually used in a CT scan to highlight the area of interest such as tumor tissues. The most commonly used contrast agent for CT scans in hospital is perhaps barium sulfate, owing to the high atomic number of barium (Z = 56). Barium sulfate is administered orally as a suspension to delineate the gastrointestinal tract using CT imaging. Despite the prevalence of the use of barium sulfate suspensions, however, this is the only example of barium as a CT contrast agent due to the high toxicity of Ba^{2+}. In this context, we propose to use BT NPs as intravenously administered cancer targeting CT contrast agents due to three main reasons according to our study: first, the HU value of BT NPs is comparable to that of barium sulfate; second, proper surface-modification of BT NPs can largely enhance their dispersibility and biocompatibility; third, the size of post-modified BT NPs can be tuned to optimal for prolonged blood circulation and tumor accumulation.

Readi-Cat 2 is an FDA-proved trademark for orally administered barium sulfate suspensions. Using a micro-CT, we compared the attenuating ability in HU between BT NPs at various concentrations and that of Readi-Cat 2 (Figure 6). As shown, for the surfactant free BT NPs in ethanol, the 30 mg/mL

concentration already exhibited higher HU (406.8) compared to Readi-Cat 2 (374.2). The HU value of the 50 mg/mL BT (870.6) was more than doubled that of Readi-Cat. For the BT@Citrate NPs in water, the higher concentrations at 40 and 50 mg/mL exhibited slightly less HU (287.9 and 289.7) than Readi-Cat (373.2). Nonetheless, these values are significantly greater than those of soft tissues, typically ranging from 20 to 100 HU. The decreased HU values of the BT@Citrate NPs compared to pristine BT NPs are likely due to the loss of Ba^{2+} during the citric acid treatment.

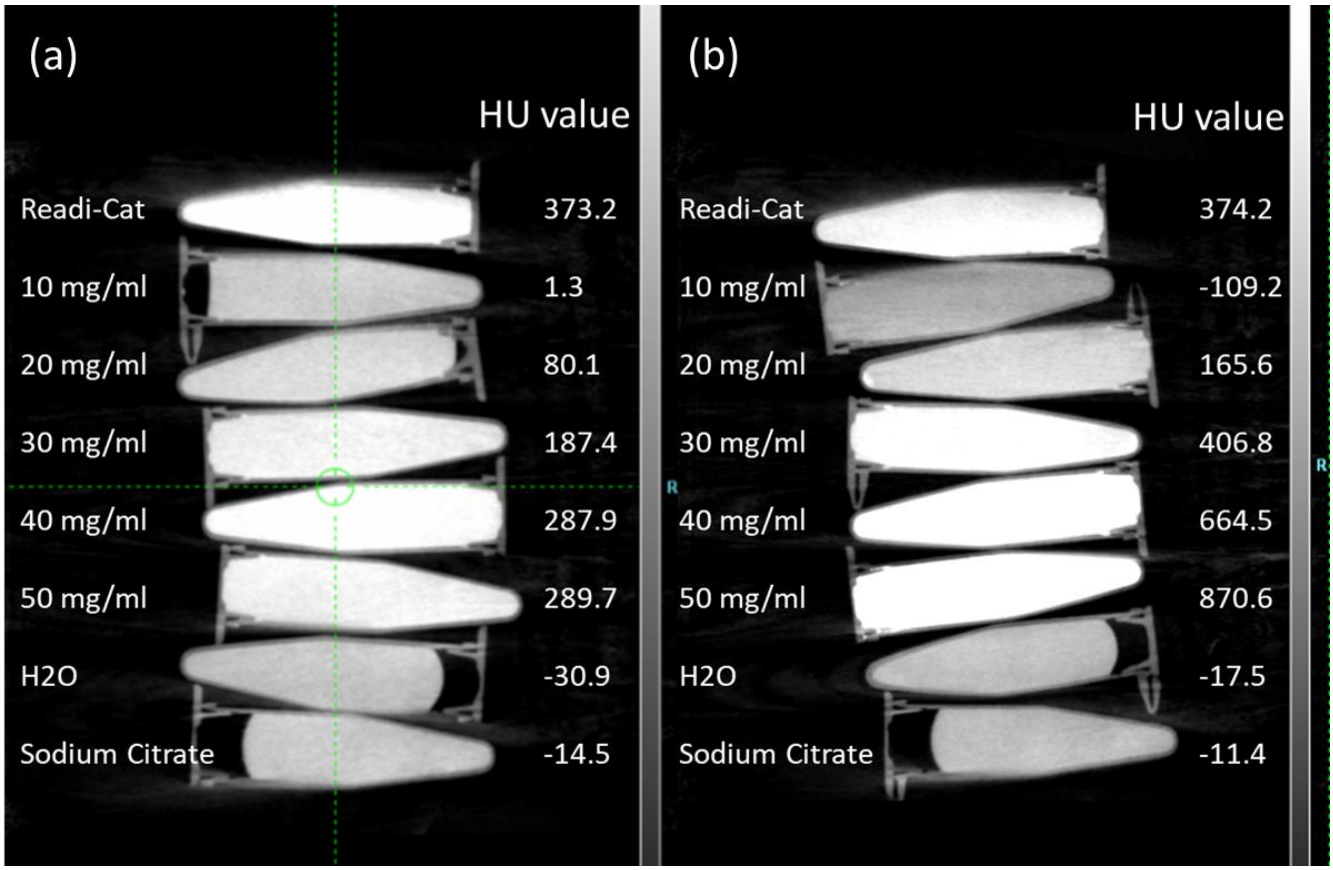

Figure 6. Micro-CT scans and HU values of BT@Citrate in water (a) and BT in ethanol (b) with various concentrations compared with Readi-Cat 2.

We also performed mouse studies using the BT@Citrate NPs by intravenously administration. Micro-CT imaging showed intensified contrast at the bladder region over time, indicating that the NPs were cleared through renal system (Supporting Information). ICP-MS results revealed that close to 80% of the

NPs were cleared by the renal system within 30 minutes (Supporting Information). As expected, the BT@Citrate NPs could not maintain long blood circulation due to the weak surface coating.

4. CONCLUSIONS

We have presented three different routes of surface modifications to enhance the aqueous dispersibility and biocompatibility of BT NPs. Our first method was to coat the BT surface with citrate molecules to produce BT@Citrate NPs. This method improved the aqueous dispersibility of BT NPs compared to non-functionalized particles. The citrate-NP adsorption can easily be disrupted causing NP aggregation by a salt concentration not yet reaching the physiological level. ## again may be better to focus on the XiO2 methods## The second modification utilized the Stöber method to produce BTNA@ SiO_2. This method produced tunable silica shell thicknesses (20-100 nm) with tunable core sizes and morphologies. ## no comment about their dispersability?## The last multi-step modification produced covalently PEGylated BT@ SiO_2 NPs with single core/shell structures. This is a multistep process that involves first an addition of an intermediate surface ligand to allow NP dispersion in a non-polar solvent, second a reverse-microemulsion technique to develop the silica layer, and third an amine functionalization for the final PEG coupling. Given the small overall size (~30 nm) and the ability to add additional functionalitis, these BT@SiO_2-PEG NPs demonstrate significant potential for biomedical applications, such targeted CT imaging.

ACKNOWLEDGEMENTS

We would like to thank Tong Wang at the Imaging Facility of CUNY Advanced Science Research Center for instrument use (TEM), scientific and technical assistance. We thank Lemin Huang at the Southern University of Science and Technology (SUSTC) for proving research facilities and advices for a summer visit. We gratefully acknowledge supports from the National Science Foundation, from NSF CREST-IDEALS, #1547830, and NSF DMR #1461499. ## I am not familiar with the funding details so I copied this from my CREST-IDEALS poster ##

REFERENCES

(1) Tassa, C.; Shaw, S. Y.; Weissleder, R. Dextran-Coated Iron Oxide Nanoparticles: A Versatile Platform for Targeted Molecular Imaging, Molecular Diagnostics, and Therapy. *Acc. Chem. Res.* **2011**, *44* (10), 842–852. https://doi.org/10.1021/ar200084x.

(2) Nguyen, K. T.; Zhao, Y. Engineered Hybrid Nanoparticles for On-Demand Diagnostics and Therapeutics. *Acc. Chem. Res.* **2015**, *48* (12), 3016–3025. https://doi.org/10.1021/acs.accounts.5b00316.

(3) Ho, D.; Sun, X.; Sun, S. Monodisperse Magnetic Nanoparticles for Theranostic Applications. *Acc. Chem. Res.* **2011**, *44* (10), 875–882. https://doi.org/10.1021/ar200090c.

(4) Lee, J. E.; Lee, N.; Kim, T.; Kim, J.; Hyeon, T. Multifunctional Mesoporous Silica Nanocomposite Nanoparticles for Theranostic Applications. *Acc. Chem. Res.* **2011**, *44* (10), 893–902. https://doi.org/10.1021/ar2000259.

(5) Tonga, G. Y.; Moyano, D. F.; Kim, C. S.; Rotello, V. M. Inorganic Nananoparticles of Therapeutic Delivery: Trials, Tribulations and Promise. *Curr. Opin. Solid State Mater. Sci.* **2014**, *19* (2), 49–55. https://doi.org/10.1038/jid.2014.371.

(6) Chen, F.; Ehlerding, E. B.; Cai, W. Theranostic Nanoparticles. *J Nucl. Med.* **2014**, *55* (12), 1919–1922. https://doi.org/10.1038/jid.2014.371.

(7) Park, K.-I.; Xu, S.; Liu, Y.; Hwang, G.-T.; L. Kang, S.-J.; Lin Wang, Z.; Jae Lee, K. Piezoelectric BaTiO3 Thin Film Nanogenerator on Plastic Substrates. *Nano Lett.* **2010**, *10* (12), 4939–4943. https://doi.org/10.1021/nl102959k.

(8) Niesz, K.; Ould-Ely, T.; Tsukamoto, H.; Morse, D. E. Engineering Grain Size and Electrical Properties of Donor-Doped Barium Titanate Ceramics. *Ceram. Int.* **2011**, *37* (1), 303–311. https://doi.org/10.1016/J.CERAMINT.2010.08.040.

(9) Lozano-Sánchez, L. M.; Lee, S. W.; Sekino, T.; Rodríguez-González, V. Practical Microwave-Induced Hydrothermal Synthesis of Rectangular Prism-like CaTiO3. *CrystEngComm* **2013**, *15* (13), 2359–2362. https://doi.org/10.1039/c3ce27040h.

(10) Huang, L.; Chen, Z.; Wilson, J. D.; Banerjee, S.; Robinson, R. D.; Herman, I. P.; Laibowitz, R.;

O'Brien, S. Barium Titanate Nanocrystals and Nanocrystal Thin Films: Synthesis, Ferroelectricity, and Dielectric Properties. *J. Appl. Phys.* **2006**, *100* (3). https://doi.org/10.1063/1.2218765.

(11) K. Dutta, P.; R. Gregg, J. Hydrothermal Synthesis of Tetragonal Barium Titanate (BaTiO3). *Chem. Mater.* **2002**, *4* (4), 843–846. https://doi.org/10.1021/cm00022a019.

(12) Paniagua, S. A.; Kim, Y.; Henry, K.; Kumar, R.; Perry, J. W.; Marder, S. R. Surface-Initiated Polymerization from Barium Titanate Nanoparticles for Hybrid Dielectric Capacitors. *ACS Appl. Mater. Interfaces* **2014**, *6* (5), 3477–3482. https://doi.org/10.1021/am4056276.

(13) Genchi, G. G.; Marino, A.; Rocca, A.; Mattoli, V.; Ciofani, G. Barium Titanate Nanoparticles: Promising Multitasking Vectors in Nanomedicine. *Nanotechnology* **2016**, *27* (23). https://doi.org/10.1088/0957-4484/27/23/232001.

(14) Ciofani, G.; Danti, S.; D'Alessandro, D.; Moscato, S.; Petrini, M.; Menciassi, A. Barium Titanate Nanoparticles: Highly Cytocompatible Dispersions in Glycol-Chitosan and Doxorubicin Complexes for Cancer Therapy. *Nanoscale Res. Lett.* **2010**, *5* (7), 1093–1101. https://doi.org/10.1007/s11671-010-9607-0.

(15) Ĉulić-Viskota, J.; Dempsey, W. P.; Fraser, S. E.; Pantazis, P. Surface Functionalization of Barium Titanate SHG Nanoprobes for in Vivo Imaging in Zebrafish. *Nat. Protoc.* **2012**, *7* (9), 1618–1633. https://doi.org/10.1038/nprot.2012.087.

(16) Jordan, T.; O'Brien, M. A.; Spatarelu, C.-P.; Luke, G. P. Antibody-Conjugated Barium Titanate Nanoparticles for Cell-Specific Targeting. *ACS Appl. Nano Mater.* **2020**. https://doi.org/10.1021/acsanm.0c00019.

(17) Rajabi, A. H.; Jaffe, M.; Arinzeh, T. L. Piezoelectric Materials for Tissue Regeneration: A Review. *Acta Biomater.* **2015**, *24*, 12–23. https://doi.org/10.1016/j.actbio.2015.07.010.

(18) Bagchi, A.; Meka, S. R. K.; Rao, B. N.; Chatterjee, K. Perovskite Ceramic Nanoparticles in Polymer Composites for Augmenting Bone Tissue Regeneration. *Nanotechnology* **2014**, *25* (48). https://doi.org/10.1088/0957-4484/25/48/485101.

(19) Tsoi, K. M.; Macparland, S. A.; Ma, X. Z.; Spetzler, V. N.; Echeverri, J.; Ouyang, B.; Fadel, S. M.; Sykes, E. A.; Goldaracena, N.; Kaths, J. M.; et al. Mechanism of Hard-Nanomaterial Clearance by the Liver. *Nat. Mater.* **2016**, *15* (11), 1212–1221. https://doi.org/10.1038/nmat4718.

(20) Hoshyar, N.; Gray, S.; Han, H.; Bao, G. The Effect of Nanoparticle Size on in Vivo Pharmacokinetics and Cellular Interaction. *Nanomedicine* **2016**, *11* (6), 673–692. https://doi.org/10.2217/nnm.16.5.

(21) Sykes, E. A.; Chen, J.; Zheng, G.; Chan, W. C. W. Investigating the Impact of Nanoparticle Size on Active and Passive Tumor Targeting Efficiency. *ACS Nano* **2014**, *8* (6), 5696–5706. https://doi.org/10.1021/nn500299p.

(22) Albanese, A.; Tang, P. S.; Chan, W. C. W. The Effect of Nanoparticle Size, Shape, and Surface Chemistry on Biological Systems. *Annu. Rev. Biomed. Eng.* **2012**, *14* (1), 1–16. https://doi.org/10.1146/annurev-bioeng-071811-150124.

(23) Pamies, R.; Cifre, J. G. H.; Espín, V. F.; Collado-González, M.; Baños, F. G. D.; De La Torre, J. G. Aggregation Behaviour of Gold Nanoparticles in Saline Aqueous Media. *J. Nanoparticle Res.* **2014**, *16* (4). https://doi.org/10.1007/s11051-014-2376-4.

(24) Edwards, S. A.; Williams, D. R. M. Double Layers and Interparticle Forces in Colloid Science and Biology: Analytic Results for the Effect of Ionic Dispersion Forces. *Phys. Rev. Lett.* **2004**, *92* (24), 10–13. https://doi.org/10.1103/PhysRevLett.92.248303.

(25) Moore, T. L.; Rodriguez-Lorenzo, L.; Hirsch, V.; Balog, S.; Urban, D.; Jud, C.; Rothen-Rutishauser, B.; Lattuada, M.; Petri-Fink, A. Nanoparticle Colloidal Stability in Cell Culture Media and Impact on Cellular Interactions. *Chem. Soc. Rev.* **2015**, *44* (17), 6287–6305. https://doi.org/10.1039/c4cs00487f.

(26) Gupta, M. N.; Roy, I. How Corona Formation Impacts Nanomaterials as Drug Carriers. *Mol. Pharm.* **2020**, *17* (3), 725–737. https://doi.org/10.1021/acs.molpharmaceut.9b01111.

(27) Ke, P. C.; Lin, S.; Parak, W. J.; Davis, T. P.; Caruso, F. A Decade of the Protein Corona. *ACS Nano* **2017**, *11* (12), 11773–11776. https://doi.org/10.1021/acsnano.7b08008.

(28) Shannahan, J. The Biocorona: A Challenge for the Biomedical Application of Nanoparticles. *Nanotechnol. Rev.* **2017**, *6* (4), 345–353. https://doi.org/10.1515/ntrev-2016-0098.

(29) Xu, H.; Gao, L. Tetragonal Nanocrystalline Barium Titanate Powder: Preparation, Characterization, and Dielectric Properties. *J. Am. Ceram. Soc* **2003**, *86* (1), 203–205.

(30) Sun, W.; Liu, W.; Li, J. Effects of Chloride Ions on Hydrothermal Synthesis of Tetragonal

BaTiO3 by Microwave Heating and Conventional Heating. *Powder Technol.* **2006**, *166* (2), 55–59. https://doi.org/10.1016/j.powtec.2006.05.007.

(31) Zheng, H.; Zhu, K.; Wu, Q.; Liu, J.; Qiu, J. Preparation and Characterization of Monodispersed BaTiO3 Nanocrystals by Sol-Hydrothemal Method. *J. Cryst. Growth* **2013**, *363*, 300–307. https://doi.org/10.1016/j.jcrysgro.2012.11.019.

(32) Dutta, P. K.; Gregg, J. R. Hydrothermal Synthesis of Tetragonal Barium Titanate. *Chem. Mater.* **1992**, *4* (4), 843–846. https://doi.org/10.1021/cm00022a019.

(33) Kwon, S. G.; Park, B. H.; Choi, K.; Choi, E. S.; Nam, S.; Kim, J. W.; Kim, J. H. Solvothermally Synthesized Tetragonal Barium Titanate Powders Using H2O/EtOH Solvent. *J. Eur. Ceram. Soc.* **2006**, *26* (8), 1401–1404. https://doi.org/10.1016/j.jeurceramsoc.2005.02.003.

(34) Bai, H.; Liu, X. Low Temperature Solvothermal Synthesis, Optical and Electric Properties of Tetragonal Phase BaTiO3 Nanocrystals Using BaCO3 Powder. *Mater. Lett.* **2013**, *100*, 1–3. https://doi.org/10.1016/j.matlet.2013.02.106.

(35) Blanco-Lopez, M. C.; Rand, B.; Riley, F. L. The Properties of Aqueous Phase Suspensions of Barium Titanate. *J. Eur. Ceram. Soc.* **1997**, *17* (2–3), 281–287. https://doi.org/10.1016/s0955-2219(96)00116-1.

(36) Kavian, R.; Saidi, A. Sol-Gel Derived BaTiO3 Nanopowders. *J. Alloys Compd.* **2009**, *468* (1–2), 528–532. https://doi.org/10.1016/j.jallcom.2008.01.045.

(37) Reverón, H.; Aymonier, C.; Loppinet-Serani, A.; Elissalde, C.; Maglione, M.; Cansell, F. Single-Step Synthesis of Well-Crystallized and Pure Barium Titanate Nanoparticles in Supercritical Fluids. *Nanotechnology* **2005**, *16* (8), 1137–1143. https://doi.org/10.1088/0957-4484/16/8/026.

(38) Gao, Y.; Shvartsman, V. V.; Elsukova, A.; Lupascu, D. C. Low-Temperature Synthesis of Crystalline BaTiO3 Nanoparticles by One-Step "Organosol"-Precipitation. *J. Mater. Chem.* **2012**, *22* (34), 17573. https://doi.org/10.1039/c2jm33373b.

(39) Brien, S. O.; Brus, L.; Murray, C. B. Synthesis of Monodisperse Nanoparticles of Barium Titanate: Toward a Generalized Strategy of Oxide Nanoparticle Synthesis. *J. Am. Ceram. Soc* **2001**, *123* (9), 12085–12086.

(40) Mandal, T. K. Characterization of Tetragonal BaTiO3 Nanopowders Prepared with a New Soft

Chemistry Route. *Mater. Lett.* **2007**, *61* (3), 850–854. https://doi.org/10.1016/j.matlet.2006.06.006.

(41) Ji, B.; Chen, D.; Jiao, X.; Zhao, Z.; Jiao, Y. Preparation and Electrical Properties of Nanoporous BaTiO3. *Mater. Lett.* **2010**, *64* (16), 1836–1838. https://doi.org/10.1016/j.matlet.2010.05.026.

(42) Ashiri, R.; Moghtada, A.; Shahrouzianfar, A.; Ajami, R. Low Temperature Synthesis of Carbonate-Free Barium Titanate Nanoscale Crystals: Toward a Generalized Strategy of Titanate-Based Perovskite Nanocrystals Synthesis. *J. Am. Ceram. Soc.* **2014**, *97* (7), 2027–2031. https://doi.org/10.1111/jace.13023.

(43) Liu, S.; Huang, L.; Li, W.; Liu, X.; Jing, S.; Li, J.; O'Brien, S. Green and Scalable Production of Colloidal Perovskite Nanocrystals and Transparent Sols by a Controlled Self-Collection Process. *Nanoscale* **2015**, *7* (27), 11766–11776. https://doi.org/10.1039/C5NR02351C.

(44) Stöber, W.; Fink, A.; Bohn, E. Controlled Growth of Monodisperse Silica Spheres in the Micron Size Range. *J. Colloid Interface Sci.* **1968**, *26* (1), 62–69. https://doi.org/10.1016/0021-9797(68)90272-5.

(45) Han, Y.; Jiang, J.; Lee, S. S.; Ying, J. Y. Reverse Microemulsion-Mediated Synthesis of Silica-Coated Gold and Silver Nanoparticles. **2008**, No. 18, 5842–5848. https://doi.org/10.1021/la703440p.

(46) Mine, E.; Yamada, A.; Kobayashi, Y.; Konno, M.; Liz-Marzán, L. M. Direct Coating of Gold Nanoparticles with Silica by a Seeded Polymerization Technique. *J. Colloid Interface Sci.* **2003**, *264* (2), 385–390. https://doi.org/10.1016/S0021-9797(03)00422-3.

(47) Kobayashi, Y.; Inose, H.; Nakagawa, T.; Gonda, K.; Takeda, M.; Ohuchi, N.; Kasuya, A. Control of Shell Thickness in Silica-Coating of Au Nanoparticles and Their X-Ray Imaging Properties. *J. Colloid Interface Sci.* **2011**, *358* (2), 329–333. https://doi.org/10.1016/j.jcis.2011.01.058.

(48) Yi, D. K.; Selvan, S. T.; Lee, S. S.; Papaefthymiou, G. C.; Kundaliya, D.; Ying, J. Y. Silica-Coated Nanocomposites of Magnetic Nanoparticles and Quantum Dots. *J. Am. Chem. Soc.* **2005**, *127* (14), 4990–4991. https://doi.org/10.1021/ja0428863.

(49) Ding, H. L.; Zhang, Y. X.; Wang, S.; Xu, J. M.; Xu, S. C.; Li, G. H. Fe3O4@SiO2 Core/Shell Nanoparticles: The Silica Coating Regulations with a Single Core for Different Core Sizes and Shell Thicknesses. *Chem. Mater.* **2012**, *24* (23), 4572–4580. https://doi.org/10.1021/cm302828d.

(50) Yang, P.; Ando, M.; Murase, N. Highly Luminescent CdSe/Cd(x)Zn(1-x)S Quantum Dots Coated with Thickness-Controlled SiO2 Shell through Silanization. *Langmuir* **2011**, *27* (15), 9535–9540. https://doi.org/10.1021/la201213c.

(51) Yi, D. K.; Lee, S. S.; Papaefthymiou, G. C.; Ying, J. Y. Nanoparticle Architectures Templated by SiO 2/Fe 2O 3 Nanocomposites. *Chem. Mater.* **2006**, *18* (3), 614–619. https://doi.org/10.1021/cm0512979.

(52) Wu, G. W.; He, S. Bin; Peng, H. P.; Deng, H. H.; Liu, A. L.; Lin, X. H.; Xia, X. H.; Chen, W. Citrate-Capped Platinum Nanoparticle as a Smart Probe for Ultrasensitive Mercury Sensing. *Anal. Chem.* **2014**, *86* (21), 10955–10960. https://doi.org/10.1021/ac503544w.

(53) Kind, C.; Feldmann, C.; Quintilla, A.; Ahlswede, E. Citrate-Capped Cu11In9 Nanoparticles and Its Use for Thin-Film Manufacturing of Cis Solar Cells. *Chem. Mater.* **2011**, *23* (23), 5269–5274. https://doi.org/10.1021/cm2024668.

(54) Cheraghipour, E.; Javadpour, S.; Mehdizadeh, A. R. Citrate Capped Superparamagnetic Iron Oxide Nanoparticles Used for Hyperthermia Therapy. *J. Biomed. Sci. Eng.* **2012**, *05* (12), 715–719. https://doi.org/10.4236/jbise.2012.512089.

(55) Turkevich, J.; Stevenson, P. C.; Hillier, J. A Study of the Nucleation and Growth Processes in the Synthesis of Colloidal Gold. *Discuss. Faraday Soc.* **1951**, *11*, 55–75.

(56) Henglein, A.; Giersig, M. Formation of Colloidal Silver Nanoparticles: Capping Action of Citrate Arnim Henglein. *J. Phys. Chem. B* **1999**, *103* (44), 9533–9539. https://doi.org/10.1021/jp9925334.

(57) Van Blaaderen, A.; Van Geest, J.; Vrij, A. Monodisperse Colloidal Silica Spheres from Tetraalkoxysilanes: Particle Formation and Growth Mechanism. *J. Colloid Interface Sci.* **1992**, *154* (2), 481–501. https://doi.org/10.1016/0021-9797(92)90163-G.

(58) Liz-marza, L. M.; Giersig, M.; Mulvaney, P. Synthesis of Nanosized Gold - Silica Core - Shell Particles. *Langmuir* **1996**, *7463* (5), 4329–4335. https://doi.org/10.1021/la9601871.

(59) Rostro-Kohanloo, B. C.; Bickford, L. R.; Payne, C. M.; Day, E. S.; Anderson, L. J. E.; Zhong, M.; Lee, S.; Mayer, K. M.; Zal, T.; Adam, L.; et al. The Stabilization and Targeting of Surfactant-Synthesized Gold Nanorods. *Nanotechnology* **2009**, *20* (43), 434005. https://doi.org/10.1088/0957-4484/20/43/434005.

(60) Susumu, K.; Medintz, I. L.; Delehanty, J. B.; Boeneman, K.; Mattoussi, H. Modification of Poly(Ethylene Glycol)-Capped Quantum Dots with Nickel Nitrilotriacetic Acid and Self-Assembly with Histidine-Tagged Proteins. *J. Phys. Chem. C* **2010**, *114* (32), 13526–13531. https://doi.org/10.1021/jp103872j.

(61) Shen, H.; M. Jawaid, A.; T. Snee, P. Poly(Ethylene Glycol) Carbodiimide Coupling Reagents for the Biological and Chemical Functionalization of Water-Soluble Nanoparticles. *ACS Nano* **2009**, *3* (4), 915–923. https://doi.org/10.1021/nn800870r.

(62) Bartczak, D.; Kanaras, A. G. Preparation of Peptide-Functionalized Gold Nanoparticles Using One Pot EDC/Sulfo-NHS Coupling. *Langmuir* **2011**, *27* (16), 10119–10123. https://doi.org/10.1021/la2022177.

(63) Chen, Z.; Chen, H.; Hu, H.; Yu, M.; Li, F.; Zhang, Q.; Zhou, Z.; Yi, T.; Huang, C. Versatile Synthesis Strategy for Carboxylic Acid - Functionalized Upconverting Nanophosphors as Biological Labels. **2008**, No. 6, 3023–3029.

(64) Paik, U.; Yeo, J. G.; Lee, M. H.; Hackley, V. A.; Jung, Y. G. Dissolution and Reprecipitation of Barium at the Particulate BaTiO3-Aqueous Solution Interface. *Mater. Res. Bull.* **2002**, *37* (9), 1623–1631. https://doi.org/10.1016/S0025-5408(02)00820-6.

(65) Yoon, D. H.; Lee, B. I.; Badheka, P.; Wang, X. Barium Ion Leaching from Barium Titanate Powder in Water. *J. Mater. Sci. Mater. Electron.* **2003**, *14* (3), 165–169. https://doi.org/10.1023/A:1022306024907.

(66) Christau, S.; Moeller, T.; Genzer, J.; Koehler, R.; Von Klitzing, R. Salt-Induced Aggregation of Negatively Charged Gold Nanoparticles Confined in a Polymer Brush Matrix. *Macromolecules* **2017**, *50* (18), 7333–7343. https://doi.org/10.1021/acs.macromol.7b00866.

(67) Sun, M.; Liu, F.; Zhu, Y.; Wang, W.; Hu, J.; Liu, J.; Dai, Z.; Wang, K.; Wei, Y.; Bai, J.; et al. Salt-Induced Aggregation of Gold Nanoparticles for Photoacoustic Imaging and Photothermal Therapy of Cancer. *Nanoscale* **2016**, *8* (8), 4452–4457. https://doi.org/10.1039/c6nr00056h.

(68) Blanco López, M. C.; Rand, B.; Riley, F. L. Polymeric Stabilisation of Aqueous Suspensions of Barium Titanate. Part II: Effect of Polyelectrolyte Concentration. *J. Eur. Ceram. Soc.* **2000**, *20* (10), 1587–1594. https://doi.org/10.1016/S0955-2219(99)00241-1.

(69) Mornet, S.; Elissalde, C.; Hornebecq, V.; Bidault, O.; Duguet, E.; Brisson, A.; Maglione, M.

Controlled Growth of Silica Shell on Ba0.6Sr 0.4TiO3 Nanoparticles Used as Precursors of Ferroelectric Composites. *Chem. Mater.* **2005**, *17* (17), 4530–4536. https://doi.org/10.1021/cm050884r.

(70) Kalender, W. A. X-Ray Computed Tomography. *Phys. Med. Biol.* **2006**, *51* (13), 29–43. https://doi.org/10.1088/0031-9155/51/13/R03.

(71) Schambach, S. J.; Bag, S.; Schilling, L.; Groden, C.; Brockmann, M. A. Application of Micro-CT in Small Animal Imaging. *Methods* **2010**, *50* (1), 2–13. https://doi.org/10.1016/j.ymeth.2009.08.007.

(72) Ashton, J. R.; West, J. L.; Badea, C. T. In Vivo Small Animal Micro-CT Using Nanoparticle Contrast Agents. *Front. Pharmacol.* **2015**, *6* (NOV). https://doi.org/10.3389/fphar.2015.00256.

(73) Lusic, H.; Grinsta, M. W. X - Ray-Computed Tomography Contrast Agents. *Chem. Rev.* **2013**, *590*.

Table 1. Particle size and surface charge measurements by DLS.

Nanoparticles	**Particle Size (nm)**	**Zeta Potential (mV)**
BT (in ethanol)	8.3 ± 0.3	
BT@Citrate	11.4 ± 0.2	-33.1 ± 0.6
BT@OA (in cyclohexane)	21.7 ± 0.3	
BT@SiO_2	28.7 ± 2.9	-31.1 ± 0.5

BT@SiO_2-NH_2	*	32.0 ± 0.5
BT@SiO_2-PEG	~40	-16.5 ± 0.8